Mon. Not. R. Astron. Soc. **265,** 365–378 (1993)

A star orbiting around a supermassive rotating black hole: free motion and corrections due to star–disc collisions

D. Vokrouhlický[1,2] and V. Karas[2,3]

[1] *Observatoire de la Côte d'Azur, Dept. CERGA, Avenue Nicolas Copernic, F-06130 Grasse, France*
[2] *Astronomical Institute, Charles University, Švédská 8, CS-150 00 Prague, Czech Republic*
[3] *Scuola Internazionale Superiore di Studi Avanzati, Via Beirut 4, I-34014 Trieste, Italy*

Accepted 1993 May 21. Received 1993 April 21; in original form 1992 September 7

ABSTRACT

Our aim is to study the evolution of the orbit of a star under the influence of interactions with an accretion disc in an AGN. The model considered consists of a low-mass compact object orbiting a supermassive black hole and colliding periodically with the accretion disc. Approximate calculations based mostly on the Newtonian theory of gravity have been carried out by several authors, to estimate the effects of circularization of initially eccentric orbits and their dragging into the disc plane. Here, we present the first step towards a more adequate general relativistic approach in which the gravitational field of the nucleus is described by the Kerr metric. The star is assumed to move along a geodesic arc between successive interactions with an equatorial accretion disc. We solve relevant formulae for the geodesic motion in terms of elliptic integrals, and construct a fast numerical code which, after specifying details of the star–disc interaction, enables us to follow the trajectory of the star for many revolutions and study the evolution of its eccentricity and inclination with respect to the disc. Lense–Thirring precession of the orbit is potentially a very important effect for observational confirmation of the presence of a rotating black hole in the nucleus. Our approach takes effects of the Lense–Thirring precession into account with no approximation.

Key words: accretion, accretion discs – black hole physics – relativity – celestial mechanics, stellar dynamics – galaxies: active.

1 INTRODUCTION AND MOTIVATION

General interest in the study of star–disc interactions in the nuclei of galaxies has greatly increased in recent years. This is partly due to the fact that they appear important in explaining the X-ray variability of active galactic nuclei (AGN). Although it is generally believed that many galaxies, and active galaxies in particular, harbour massive black holes in their cores, there is no direct observational confirmation for this paradigm. The origin of this difficulty is apparent: the complicated plasma physics of the matter swirling around the black hole makes it difficult to distinguish the effects of general relativity – although they may be essential for the mechanism of energy generation itself. A potentially very important observable is X-ray data on the variability of active galactic nuclei (for a recent review, see Wallinder, Kato & Abramowicz 1992). Although our understanding of the origin of X-rays is not satisfactory, it is often accepted that they are generated in the inner regions of the accretion disc, where general relativistic effects are significant. When trying to describe these effects, it is useful to separate the details of the radiation-generating mechanism (described in the local frame comoving with the matter), i.e. the local physics of the interaction, from observable effects as seen by a distant observer. In our previous work (Karas, Vokrouhlický & Polnarev 1992, hereafter Paper I), we developed a code which can be used in many astrophysically relevant situations to calculate images of various effects occurring in the close vicinity of the rotating (Kerr) black hole. Our code deals efficiently with problems treated originally by Cunningham & Bardeen (1973). All relativistic effects on photons (such as gravitational and Doppler shifts of frequency, and bending of light rays) were taken into account. As an example, we applied the code to the 'hotspot' model of the periodic AGN variability. This model explains the X-ray variability on a time-scale of approximately 3 h in terms of a bright orbiting spot (or spots) located on the accretion disc (Abramowicz et al. 1992). We also discussed the case of a large number of

spots with different intrinsic characteristics, which may be relevant to an explanation of the X-ray variability of AGN on still shorter time-scales (Abramowicz et al. 1991).

In this paper we present a method for calculating the evolution of the orbital parameters of a compact star orbiting a massive black hole. Such a star may come from a binary or a cluster tidally disrupted by the central black hole (Hills 1988; Novikov, Pethick & Polnarev 1992). It can be deposited in a tightly bound orbit with a close pericentre where relativistic effects are important. The star interacts with the accretion disc only at the moment when it crosses the equatorial plane, and this interaction weakly affects its motion. Cumulative effects of successive tiny interactions circularize the trajectory and change the orbital plane into the plane of the disc. Mutual star–disc interactions were discussed by Syer, Clarke & Rees (1991) as a possible origin of the fuelling and variability of AGN. In particular, they discussed relative time-scales for circularization of the orbit and its alignment with the disc plane, and the final radius of the embedded orbit. Naturally, quantitative estimates depend on poorly known details of the interaction (cf. Zurek, Siemiginowska & Colgate 1992). A compact star colliding with an accretion disc is one of the viable models for the periodic variability of AGN (Abramowicz 1992; Sikora & Begelman 1992; Rees 1993). At present we still lack a comprehensive analysis of observational data which would suggest suitable candidates for such objects. General relativistic precession of orbital nodes (the Lense–Thirring effect) – if detected – would strongly support models of AGN that involve rotating supermassive black holes. Lense–Thirring precession affects the inclined trajectory of a star, but it has been discussed only in the special cases of free orbits with a large radius compared to the gravitational radius of the central black hole (Lense & Thirring 1918) and spherical orbits around an extreme Kerr black hole (Wilkins 1972). We consider the more general case of eccentric orbits that interact with the equatorial disc, and we do not assume any particular value of the angular momentum of the central black hole.

Star–disc interactions are a complex problem. Because we assume that the disc produces only a weak perturbation of free motion of the star, we can attack the problem in several steps. The present paper concentrates on an effective method for calculating the free motion of the star between its successive interactions with the disc. Simple examples of how star–disc interactions may change the picture are given in the final section, and they will be discussed in a forthcoming paper in greater detail. Detailed calculation of the Lense–Thirring frequency relevant for this model will be given elsewhere (Karas & Vokrouhlický 1993). Once the motion of the star and its interaction with the disc are specified, we can apply the method of Paper I to compute the shape of the light curve or resultant spectrum (see also Cunningham & Bardeen 1973; Luminet 1979; Laor & Netzer 1989). Recently, Fabian et al. (1989), Kojima (1991) and Laor (1991) applied an analogous approach to study line profiles from accretion discs. For a more complete list of references, see Paper I.

Let us briefly describe the configuration of the model. We consider a low-mass compact object (white dwarf, neutron star or black hole) orbiting the central massive black hole of the AGN. In our approach, we restrict ourselves to the assumption that the orbiting object moves along a time-like geodesic in the unperturbed background Kerr metric outside the equatorial plane. Thus we implicitly assume that (i) the orbiting object is sufficiently compact and/or far from the central black hole (we neglect any coupling of the higher multipoles of the star to the background curvature), and (ii) its mass is very small compared to the mass of the central black hole (we do not consider perturbations of the background metric). We also neglect the influence of radiating gravitational waves. In several astrophysical situations, such assumptions may not be appropriate – see, for example, Carter & Luminet (1983), Luminet & Marck (1985) and Carter (1992), who studied tidal squeezing of the stars by the nearby black hole. Thorne & Hartle (1985) and Suen (1986) developed a scheme for multipole-tidal interactions of relativistic objects. For the motion of black holes that are close in distance and comparable in mass, see, for example, D'Eath (1975a, b). We do not consider such extreme situations in this paper. Kates (1980) has shown that the star will move very nearly along a geodesic in the unperturbed background metric for a sufficiently long time, provided that the ratio of its mass and the characteristic reference length of the background metric is small. We have in mind situations where this parameter is of the order of 10^{-5} or even less. This is important to note, because we will attempt to follow the trajectory of the orbiting object for long periods of time. Next, we assume that the accretion disc is in the equatorial plane of the central black hole. We exclude thick-disc models from our present considerations. Each time the object crosses the equatorial plane, it interacts with the disc (provided that the intersection is between the outer and the inner edges of the disc). In other words, we assume that the trajectory consists of arcs of free geodesic motion above (or below) the disc plane and impulsive changes of the orbital parameters at the moment of passage through the disc. The whole 'physics' of the problem is compressed into the prescription governing the changes of the orbital parameters when crossing the equatorial plane. The interaction is assumed to be very weak, which implies that relative changes of energy, angular momentum and other quantities characterizing the orbit of the star are much less than unity in each single event. We should note that the geodesic motion in the Kerr space–time is integrable; thus a strong dependence of the shape of the orbit on initial conditions, which is typical for chaotic motion, cannot be expected in the Kerr space–time. An alternative approach, which employs a statistical description with appropriately averaged quantities, is in preparation. The separation of dynamical and physical aspects, which we introduce in the present paper, appears to be very advantageous, and it allows us to employ a fast method to compute the evolution of the orbital parameters.

2 THE MAPPING: DETAILS OF THE CALCULATION

We consider the geodesic motion of a test particle (representing a star or a low-mass black hole) in the fixed Kerr background metric. We are interested only in short arcs of geodesic motion, with the following boundary conditions: the initial point (indexed 'i') lies in the equatorial plane ($\theta=\pi/2$ in Boyer–Lindquist coordinates); the final point (indexed 'f') is the nearest successive intersection of the orbit with the equatorial plane. We employ a 'mapping', by which we mean

an analytical algorithm to evaluate the final position (r_f, ϕ_f) from the initial position (r_i, ϕ_i) with constants of motion assumed to be given. In applications, we also need to know the transformation from initial to final velocities dr/dt, $d\theta/dt$ and $d\phi/dt$ to obtain the full starting information for the physical model of the interaction of the orbiting object with the accretion disc. The whole procedure is trivial in principle, because the geodesic motion is separable in the Kerr background metric and the equations of motion can be reduced to a set of ordinary first-order differential equations (Carter 1968). Our main task is to handle the problem efficiently.

Carter's equations involve squares of the velocities. As the star crosses the equatorial plane, the latitudinal velocity changes its sign periodically. In order to treat the case of the radial velocity, we introduce the sign function $\eta \equiv \mathrm{sgn}(dr/dt)$. Thus our mapping is the analytical transformation

$$(r, \phi; \eta)_i \xrightarrow{M} (r, \phi; \eta)_f.$$

We will also be interested in analytical evaluation of the delay in coordinate time that is necessary to pass from the initial to the final configuration in the disc plane: $(t_f - t_i)$. In particular, this is important for reconstruction of the AGN photometric curve, provided that its variability arises from similar periodic processes to those described here (star–disc interactions) (Karas & Vokrouhlický 1993).

It is worth noting that the code based on this mapping technique is optimized as far as *both* the speed and the accuracy are concerned. The effective step of the method is the whole orbital arc, and it cannot, in principle, be made greater. Moreover, the exact analytical solution of the problem is chosen as a sample function covering one integration step (instead of, for example, polynomials in Runge–Kutta methods). We remark that the name 'mapping' comes from analogous methods developed in celestial mechanics (e.g. Wisdom 1982; Murray 1986).

We use the standard notation for the Kerr metric (Bardeen 1973). Quantities with the dimension of length in geometrized units are divided by the mass of the central black hole, M, and they are thus made dimensionless. Time-like geodesics in the Kerr space–time can be integrated in the form

$$t_f - t_i = \int_{r_i}^{r_f} \frac{r^2(r^2+a^2)\,\mathscr{E} + 2ar(a\mathscr{E} - \Phi)}{\Delta R(r)^{1/2}}\,dr + \int_{\theta_i}^{\theta_f} \frac{a^2\mathscr{E}\cos^2\theta}{\Theta(\theta)^{1/2}}\,d\theta, \tag{1}$$

$$\phi_f - \phi_i = \int_{r_i}^{r_f} \frac{r^2\Phi + 2r(a\mathscr{E} - \Phi)}{\Delta R(r)^{1/2}}\,dr + \int_{\theta_i}^{\theta_f} \frac{\Phi\cot^2\theta}{\Theta(\theta)^{1/2}}\,d\theta, \tag{2}$$

$$\int_{r_i}^{r_f} \frac{dr}{R(r)^{1/2}} = \int_{\theta_i}^{\theta_f} \frac{d\theta}{\Theta(\theta)^{1/2}} \tag{3}$$

(Carter 1968). Here,

$$R(r) = (\mathscr{E}^2 - 1)\,r^4 + 2r^3 + [(\mathscr{E}^2 - 1)\,a^2 - \Phi^2 - Q]\,r^2 + 2\mathscr{K}r - a^2 Q, \tag{4}$$

$$\Theta(\theta) = Q - [a^2(1 - \mathscr{E}^2) + \Phi^2 \sin^{-2}\theta]\cos^2\theta,$$

$$Q = \mathscr{K} - (\Phi - a\mathscr{E})^2, \tag{5}$$

and

$$\Sigma = r^2 + a^2\cos^2\theta, \qquad \Delta = r^2 + a^2 - 2r,$$

$$A = (r^2 + a^2)^2 - \Delta a^2 \sin^2\theta.$$

The constants of motion, $\mathscr{E} = -p_t$, $\Phi = p_\phi$ and $\mathscr{K}$, can be expressed in terms of components of the four-momentum in the locally non-rotating frame (LNRF):

$$\mathscr{E} = \left[\left(\frac{\Sigma\Delta}{A}\right)^{1/2} p^{\hat{t}} + \frac{2ar}{(\Sigma A)^{1/2}}\,p^{\hat{\phi}}\right]_{r_i,\,\theta_i = \pi/2},$$

$$\Phi = \left[\left(\frac{A}{\Sigma}\right)^{1/2} p^{\hat{\phi}}\right]_{r_i,\,\theta_i = \pi/2}, \tag{6}$$

$$\mathscr{K} = [(\Phi - a\mathscr{E})^2 + \Sigma(p^{\hat{\theta}})^2]_{r_i,\,\theta_i = \pi/2}. \tag{7}$$

Components of the four-momentum in terms of direction cosines in the local sky of an observer at rest with respect to the LNRF are

$$p^{\hat{t}} = \gamma, \qquad p^{\hat{r}} = \gamma v\cos\alpha, \qquad p^{\hat{\theta}} = \gamma v\sin\alpha\cos\beta,$$

$$p^{\hat{\phi}} = \gamma v\sin\alpha\sin\beta, \tag{8}$$

where v is the tetrad velocity of the particle in the LNRF, and the Lorentz factor

$$\gamma = \frac{1}{\sqrt{1 - v^2}}.$$

Specification of the initial conditions as a result of the star–disc interaction in the local frame comoving with the disc matter requires another boost to the disc corotating frame (DCF). In the case of a Keplerian thin disc in the equatorial plane, the linear velocity of the DCF with respect to the LNRF is

$$v_{\mathrm{DCF}} = \frac{r^2 - 2ar^{1/2} + a^2}{(r^{3/2} + a)\,\Delta}.$$

It is known that integrals (1)–(3) can be reduced to standard elliptic integrals, but only the simplest cases have been discussed in the literature. The explicit form of relevant formulae depends on the values of the constants of motion and initial conditions. We shall restrict ourselves to the most interesting astrophysical case: stable, energetically bound trajectories that cross the equatorial plane many times repeatedly. Thus we assume $0 < \mathscr{E} < 1$. We exclude singular cases of orbits lying exactly in the equatorial plane ($Q = 0$: Bardeen, Press & Teukolsky 1972), or those intersecting the rotational axis ($\Phi = 0$: Stoghianidis & Tsoubelis 1987); we also exclude the case of the very fast rotating black hole, $a = 1$. In the Schwarzschild case ($a = 0$) the geodesic is always planar, while $a \neq 0$ leads to the Lense–Thirring precession of the orbit and we have to take into consideration the dragging of the nodes [Wilkins (1972) discussed this effect for spherical orbits in the extreme Kerr case].

First, we simplify the integrals (1)–(3) to a form that can be directly found in standard tables of elliptical integrals (Gröbner & Hofreiter 1965; Byrd & Friedman 1971; Gradshteyn & Ryzhik 1980). For this purpose, we need to find the roots of $R(r)$ and $\Theta(\theta)$. The real roots are the turning

points of the radial and latitudinal motions, respectively. We specify the initial point of the geodesic as $(t_i, r_i, \pi/2, \phi_i)$, and we look for the final position $(t_f, r_f, \pi/2, \phi_f)$ which is in the equatorial plane again. The polynomial $R(r)$ governing the radial motion is of the fourth order, with $R(r_i) \geq 0$. In our case, $R(r) < 0$ for $r \to \infty$ and $r = 0$. Thus we can find two real roots, $r_A \in (0, r_i)$ and $r_B \in (r_i, \infty)$, and for the remaining two roots we obtain the quadratic equation

$$(\mathscr{E}^2 - 1)\, r^2 + [(\mathscr{E}^2 - 1)(r_A + r_B) + 2]\, r - \frac{a^2 Q}{r_A r_B} = 0. \tag{9}$$

Supposing that all roots are real we can denote them, in a descending sequence, as $r_1 > r_2 > r_3 > r_4$. We exclude the possibilities of multiple roots because such situations are singular in the sense that they occur for precisely arranged values of $\mathscr{E}$ and Φ. The probability that interaction with the accretion disc will lead to such values is zero (in the measure sense). Thus we have

$$I_r \equiv \int \frac{\mathrm{d}r}{R(r)^{1/2}} = \frac{1}{\sqrt{1-\mathscr{E}^2}} \int \frac{\mathrm{d}r}{\sqrt{|(r-r_1)(r-r_2)(r-r_3)(r-r_4)|}}. \tag{10}$$

In the case of two real and two complex roots ($r_1 > r_2$ and r_3, $\overline{r_3}$, respectively), we obtain

$$I_r = \frac{1}{\sqrt{1-\mathscr{E}^2}} \int \frac{\mathrm{d}r}{(r_1 - r)(r - r_2)\sqrt{(r-\chi_1)^2 + \chi_2^2}}, \tag{11}$$

where

$$\chi_1 = \mathrm{Re}(r_3), \qquad \chi_2 = \mathrm{Im}(r_3).$$

The latitudinal motion is governed by the polynomial $\Theta_\mu(\mu) \equiv \sin^2\theta\,\Theta(\theta)$ (equation 5). Solving the bi-quadratic equation in $\mu \equiv \cos\theta$,

$$a^2(1-\mathscr{E}^2)\,\mu^4 - [Q + a^2(1-\mathscr{E}^2) + \Phi^2]\,\mu^2 + Q = 0, \tag{12}$$

we obtain the roots $\mu_+ > \mu_- > 0$. The latitudinal motion is only possible in the region $\mu \in \langle -\mu_-, \mu_- \rangle$, and

$$I_\mu \equiv \int \frac{\mathrm{d}\mu}{\Theta_\mu(\mu)^{1/2}} = \frac{1}{a\sqrt{1-\mathscr{E}^2}} \int \frac{\mathrm{d}\mu}{\sqrt{(\mu_+^2 - \mu^2)(\mu_-^2 - \mu^2)}}. \tag{13}$$

Analogously, the azimuthal motion can be solved in the form

$$\phi_f - \phi_i = [2(a\mathscr{E} - \Phi)\,A_+ + \Phi B_+]\, I_+ + [2(a\mathscr{E} - \Phi)\,A_- + \Phi B_-]\, I_- + \Phi J_\mu, \tag{14}$$

where

$$I_\pm = \int \frac{\mathrm{d}r}{(r - r_\pm)\,R(r)^{1/2}}, \qquad J_\mu = \int \frac{\mathrm{d}\mu}{(1-\mu^2)\,\Theta_\mu(\mu)^{1/2}},$$

$$A_\pm = \pm \frac{r_\pm}{r_+ - r_-}, \qquad B_\pm = \pm \frac{2r_\pm - a^2}{r_+ - r_-},$$

$$r_\pm = 1 \pm \sqrt{1 - a^2}. \tag{15}$$

Finally, for the time coordinate we obtain

$$t_f - t_i = \mathscr{E}(J_r + 2K_r) + 2[B_+ r_+ \mathscr{E} + a(a\mathscr{E} - \Phi)\,A_+]\, I_+ + 2[B_- r_- \mathscr{E} + a(a\mathscr{E} - \Phi)\,A_-]\, I_- + 4\mathscr{E} I_r + a^2 \mathscr{E} K_\mu, \tag{16}$$

with

$$J_r \equiv \int \frac{r^2\,\mathrm{d}r}{R^{1/2}}, \qquad K_r \equiv \int \frac{r\,\mathrm{d}r}{R^{1/2}}, \qquad K_\mu \equiv \int \frac{\mu^2\,\mathrm{d}\mu}{\Theta_\mu(\mu)^{1/2}}. \tag{17}$$

It is straightforward but moderately tedious to derive the explicit form of the mapping. We give relevant formulae in Appendix A.

3 THE EVOLUTION OF ORBITS: SIMPLE EXAMPLES

There are several interesting issues closely related to our problem that have not as yet been fully understood. In this section we present simple examples of secular changes of the orbital parameters of a star orbiting a supermassive (10^6–10^9 $M_\odot$) black hole and interacting with the accretion disc. In particular, we study the eccentricity and inclination of the orbit, as they are introduced in Appendix A. Differences from previous estimates that have been made within the framework of Newtonian gravity are found to be significant for nearly unstable orbits. These differences can be very subtle and can interfere with the details of the star–disc interaction, and thus at first we adopted an extremely simplified (and perhaps unrealistic) description of the interaction. The Lense–Thirring precession of the orbit was included fully relativistically, with no approximation. This is important for the particular example that we discuss below. The mass of the black hole is assumed to be about 10^7 $M_\odot$, for definiteness. This means that the periodicity of the modulation of the X-ray emission on a time-scale of several hours corresponds to a radius of the orbit a factor of a few tens greater than the gravitational radius of the black hole – rather close to the horizon where approximation methods for the Lense–Thirring precession are no longer satisfactory. We should note, for completeness, that, if the star–disc interaction is switched off, the eccentricity of the orbit remains constant in time and the value of the precession is exactly that of the Lense–Thirring precession.

In the following examples, we tune the strength of the star–disc interaction in such a way that the relative change of orbital parameters is of the order of $\approx 10^{-5}$ in each interaction, and we follow $\approx 10^5$ revolutions. Each of the following figures shows the sequence of radial coordinates r for successive intersections of the trajectory with the disc – one point corresponds to one intersection, while two intersections correspond to one revolution of the star. (Alternatively, instead of the number of intersections N we could use coordinate time t to label the x-axis; the figures remain very similar in shape, but this alternative possibility appears more adequate for plotting computed light curves which should be related to the observer's time at infinity.) The upper and lower boundaries of the distribution of intersections are current values of the apocentre and the pericentre, respectively. Intersections are (seemingly randomly) scattered in the whole range between these boundaries, due to the shift of the pericentre and Lense–Thirring precession (if $a \neq 0$). Fre-

quencies corresponding to both of these effects are quantitatively studied by Karas & Vokrouhlický (1993).

In the first example we assume that, as a result of the interaction, the *difference* in the azimuthal components of the star and the disc material (evaluated in the DCF) is reduced:

$$\Delta v_{\phi,\mathrm{DCF}} \longrightarrow \alpha_* \Delta v_{\phi,\mathrm{DCF}}, \tag{18}$$

where α_* is a phenomenological parameter $\lesssim 1$. Initially retrograde orbits (those with $I > 90°$) decrease the absolute magnitude of their Φ-component of angular momentum due to interactions with the disc, and they either get captured by the black hole or become prograde. Once they are prograde, the star acquires angular momentum from the disc and moves away from the black hole. Simultaneously, both the eccentricity and the inclination decrease, and the orbital period increases. The effect of energy dissipation due to crashing through the disc is not considered in equation (18). The model is of course inadequate when the inclination reaches zero and the star becomes a part of the disc. Fig. 1 is an example of such an orbit. As mentioned above, the unperturbed geodesic motion in the Kerr metric is integrable, and thus we do not expect the characteristic time for circularization or changing of the trajectory to the disc plane to depend on particular values of the initial position or directions of velocity of the star.

Our second example is a modification of the model studied by Syer et al. (1991). It is complementary to the previous one because energy dissipation is now considered, while the difference in azimuthal velocity of the star relative to the disc material is ignored. We suppose that the star hits the disc supersonically and draws some of the material, with a mass $\Delta m \approx \rho_{\mathrm{disc}} h_{\mathrm{disc}} A_{\mathrm{eff}} \sin^{-1} I$, out of the disc; here, ρ_{disc} and h_{disc} are the local density and thickness of the disc, respectively, and A_{eff} is the effective cross-section for the star–disc interaction. The energy dissipated during the interaction is proportional to the kinetic energy acquired by the disc material, $\Delta \mathscr{E}_{\mathrm{diss}} \propto \Delta m(\gamma_{\mathrm{DCF}} - 1)$. We assume that the acceleration of the star that results from this interaction is antiparallel to the velocity of the star, and the corresponding change of the velocity is

$$\Delta \boldsymbol{v} = -\frac{\Delta \mathscr{E} \boldsymbol{v}}{m_* \gamma_{\mathrm{DCF}}^3 v^2} \propto -\frac{\rho_{\mathrm{disc}} h_{\mathrm{disc}} A_{\mathrm{eff}} (\gamma_{\mathrm{DCF}} - 1)\, \boldsymbol{v}}{m_* \gamma_{\mathrm{DCF}}^3 v^2 \sin I}. \tag{19}$$

(We should note that the last equation for the star–disc drag becomes inappropriate and must be modified when the motion of the star is subsonic and the disc material is directly accreted on to the star. The motion is highly supersonic, with a Mach number of the order of 10^2–10^3, under the conditions that we consider.) Naturally, ρ_{disc} and h_{disc} depend on the disc model. Because we do not want to enter into these additional details, we assume that they, as well as A_{eff}, are constant. [We have also carried out computations using the density profiles corresponding to the Novikov & Thorne (1973) relativistic thin-disc model, which yield only

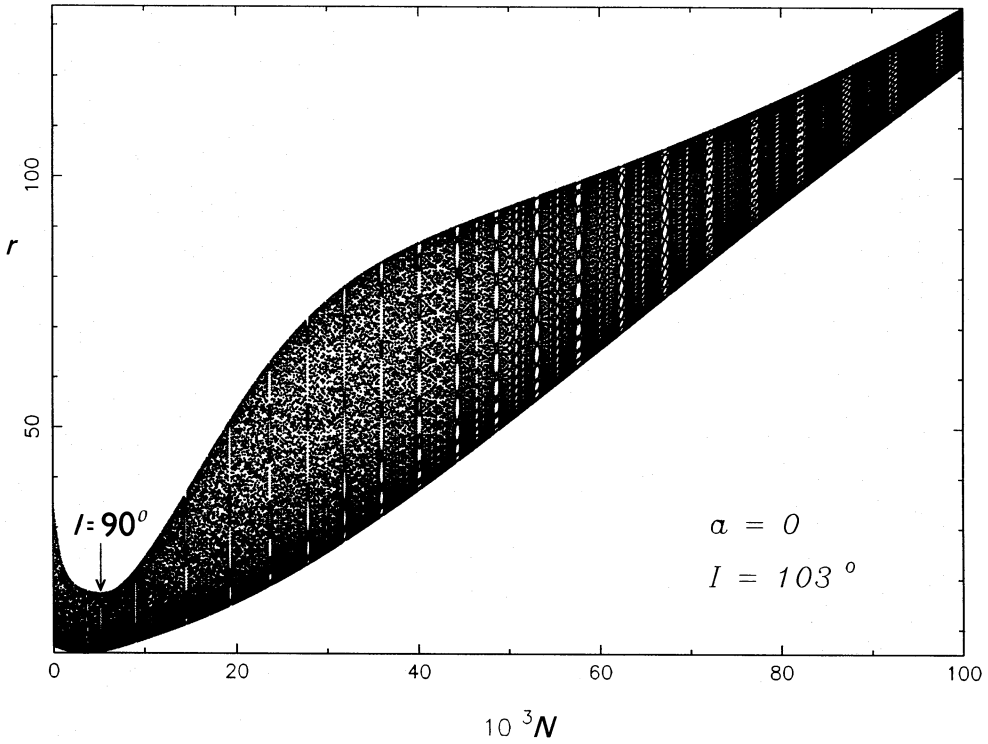

Figure 1. The sequence of successive intersections with the disc. We plot the radial coordinate r of the intersection on the ordinate and the number of intersections N on the abscissa. For $N \gtrsim 5 \times 10^4$ the upper and lower boundaries of the distribution of intersections in the figure get closer to each other, which means that the eccentricity of the orbit decreases; simultaneously, as the orbit is circularized it is also dragged into the plane of the disc. In this case, $a = 0$ and $\alpha_* = 0.9999$. The initial pericentric distance is 7, the eccentricity is 0.7, and the inclination $I = 103°$. The arrow indicates the moment when the orbit changes its character from retrograde to prograde ($I = 90°$).

moderate modifications to the results.] Fig. 2 illustrates two typical cases – both orbits are initially prograde with (a) $I = 35°$ and (b) $I = 80°$. In general, the final radius of the orbit can be either larger (for small values of the initial inclination) or smaller (for large values) than the initial pericentre. We find that initially retrograde orbits became captured in this model. This feature can be naturally explained as follows. Dissipation of the orbital energy during each intersection with the disc tends to increase the binding energy of the orbiting object. In the case of originally prograde orbits,

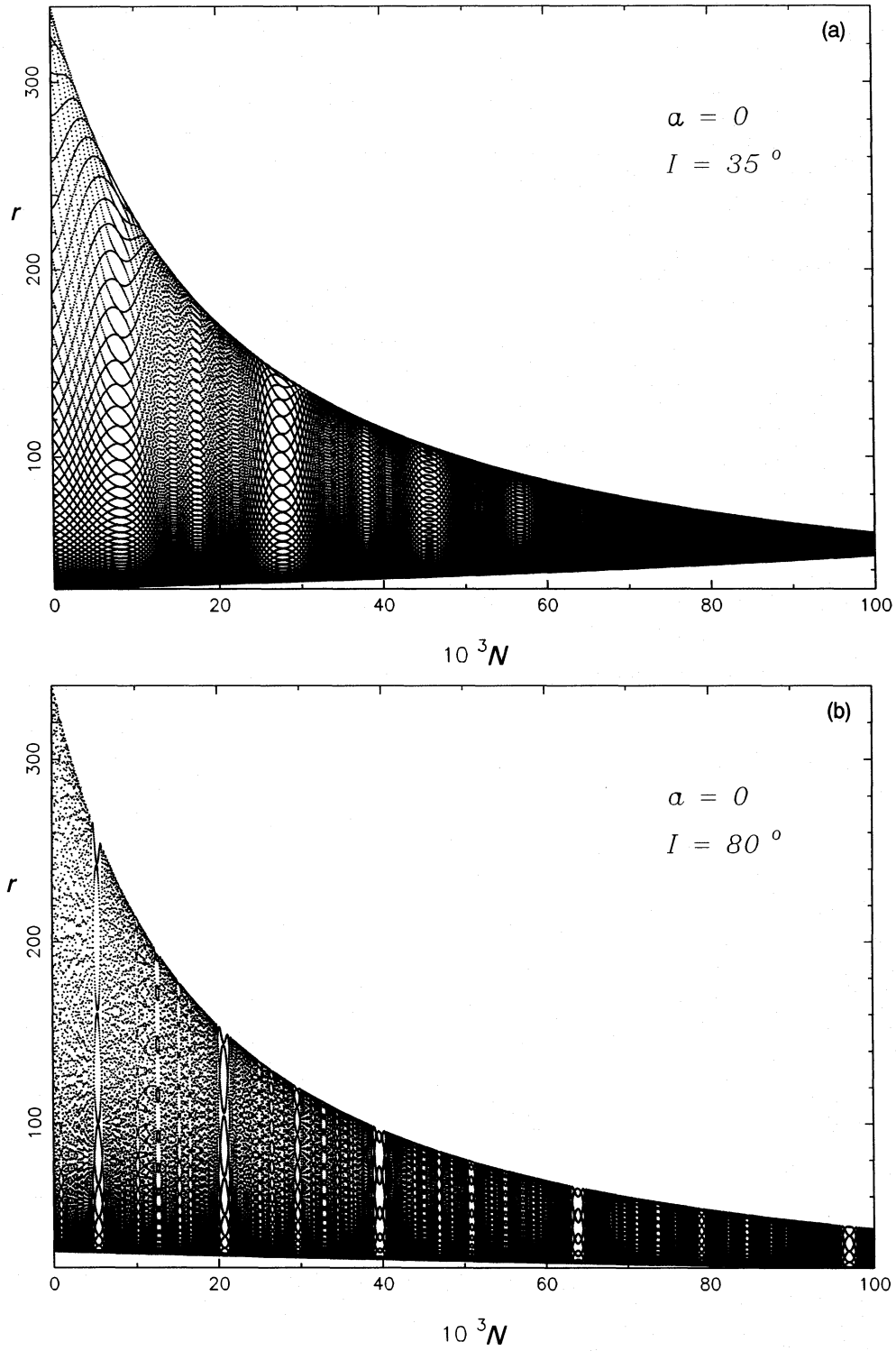

Figure 2. As in Fig. 1, but for the second model of the star–disc interaction (equation 40). The initial pericentric distance is 30 and the eccentricity $e = 0.83$. Two initial inclinations are compared: (a) $I = 35°$, (b) $I = 80°$. The proportionality constant in (40) is taken as 10^{-5}. The originally less inclined orbit (a) settles on the circular orbit in the disc with a radius of ≈ 53, while the more inclined orbit (b) becomes circularized at a radius of ≈ 17.7. We have verified, as an example, that if the initial pericentre is kept at 30 the results are not very sensitive to the initial eccentricity, provided that it is $\gtrsim 0.75$.

however, the orbiting object gains a sufficient amount of angular momentum, which saves it from being captured by the black hole. Finally, the object settles into a circular orbit in the disc plane. An object that started with a retrograde orbit, however, does not acquire enough angular momentum during the period of nearly perpendicular intersections with the disc. Due to continuous losses of energy, it is typically captured by the hole.

To clarify previous results based on the relativistic treatment, we have compared them with the corresponding Newtonian 'elliptic' mapping (see Appendix A). To be consistent, we have also reduced the formulae for the star–disc interaction by eliminating the Lorentz factor $\gamma_{\rm DCF}$ in (19), and, instead of the Lorentz boost from the LNRF to the DCF, we have used the Galilean transformation. Fig. 3(a) shows the fully relativistic model with the Schwarzschild background metric, while Fig. 3(b) is the Newtonian analogue. We have chosen formally the same initial eccentricity and inclination in both figures: $e \simeq 0.83$ and $I = 130°$. The orbit is initially retrograde and in the relativistic case it is captured by the central black hole. In contrast, this does not occur in the Newtonian case, and the orbit is circularized to some definite radius. (In a realistic case, however, the orbiting object can be tidally disrupted before it is captured, but this depends on its internal structure and we do not consider such a possibility in the present paper.) Because the interaction of the orbiting object with the disc is always chosen to be weak, the time-scale for the precession of the pericentre is much shorter than the time-scale for the evolution of the other orbital parameters. As a consequence, the points of intersection with the disc fill the interval between the current pericentre and the apocentre in the relativistic case (Fig. 3a). There is no precession of the pericentre in the Newtonian case, and thus only an 'adiabatic' evolution of the orbital parameters is seen (Fig. 3b).

We also show the results of an integration with the nearly extreme Kerr black hole. In this example, we have chosen $a = 0.9981$ for definiteness (Thorne 1974), the same initial eccentricity and inclination, and the same initial apocentre and pericentre (expressed in units of gravitational radii) as in Fig. 2. We observe (Fig. 4) a slightly shorter circularization time than in the corresponding Schwarzschild case, but the qualitative features of the disc–orbit interaction remain unchanged. They may be changed, however, when details of the structure of the accretion disc are taken into account, because the structure of the disc and the location of its inner edge depend significantly on a. Again, we find that initially retrograde orbits get captured by the black hole.

4 CONCLUSIONS

We have assumed that the low-mass compact object interacts with the thin accretion disc twice per revolution – exactly when it crosses the equatorial plane of the black hole (the impulsive approximation). We have described the relevant equations and we have employed them in a fast numerical code to compute the evolution of the trajectory. We have found that the effective time of circularization is shorter than the time to change the orbital plane into the plane of the disc. This conclusion is in accordance with the previous results of Syer et al. (1991), based on Newtonian gravity. However, we have also observed short periods during the evolution when eccentricity increases. In particular, this increase occurs in the model described by equation (18) during the transition period when the initially retrograde character of the orbit is changed to a prograde one.

The star–disc interaction is described by a phenomenological parameter characterizing the magnitude of the change of orbital parameters in each collision. This phenomenological description is satisfactory provided that the disc remains thin and the orbital parameters are changed only at the moment of transition of the star through the equatorial plane of the central black hole. A description of the interaction that would result from a detailed physical model is not crucial in this case; we want to improve our understanding of the interaction in future work. Effects of the dynamical friction and direct accretion acting on an object moving through the gaseous medium have been studied by a number of authors under various conditions (recently by Petrich et al. 1989). In our highly supersonic and turbulent case, the approach outlined by Zurek et al. (1992) appears to be the most appropriate one.

One can specify parameters of the model for the case of NGC 6814. Each single long-duration observation by *EXOSAT* or *Ginga* covers less than 30 revolutions of the orbiting object. The characteristic time-scale for the precession of nodes is much longer than the orbital one. The estimate that adopts the maximum value of $a = 1$ and a radius of the orbit of 50 gravitational radii of the central black hole yields a ratio of the Lense–Thirring to the orbital frequency of ≈ 0.005. This means that the orientation of the orbit is not significantly changed during each observation. However, the interval between *EXOSAT* observations and *Ginga* observations was certainly long enough, and a resulting change in the orientation would suggest an opportunity to understand the perfect stability of the orbital period detected by both satellites and, at the same time, the puzzling change in the light-curve profile. We do not want to speculate further on this important subject until more reliable data are available. Star–disc collisions are presumably crucial for the theory of all AGN that harbour a dense star cluster in their core.

To conclude, adopting the model of star–disc interactions as an explanation of the origin of the periodically variable light curve, we see one important contribution from general relativistic effects which is due to the pericentric shift and Lense–Thirring precession. These effects drag the point on the orbit where the star crashes through the disc. They also modify the velocity at which the star hits the disc, as well as the orientation of the orbit with respect to the observer. This fact has two consequences: (i) additional periodicities corresponding to the precession frequencies are present, and can potentially be revealed in the power spectrum of the signal from the source (Karas & Vokrouhlický 1993); (ii) long-term evolution of marginally stable and marginally bound orbits is very different from that of orbits with identical initial parameters treated in the Newtonian theory of gravity. The first consequence above suggests that it may be possible to detect Lense–Thirring precession induced near the core of an AGN. If the corresponding frequency is not present, we will be able to conclude that the central black hole (if any) is non-rotating. This would be extremely important information, especially from the point of view of electromagnetic

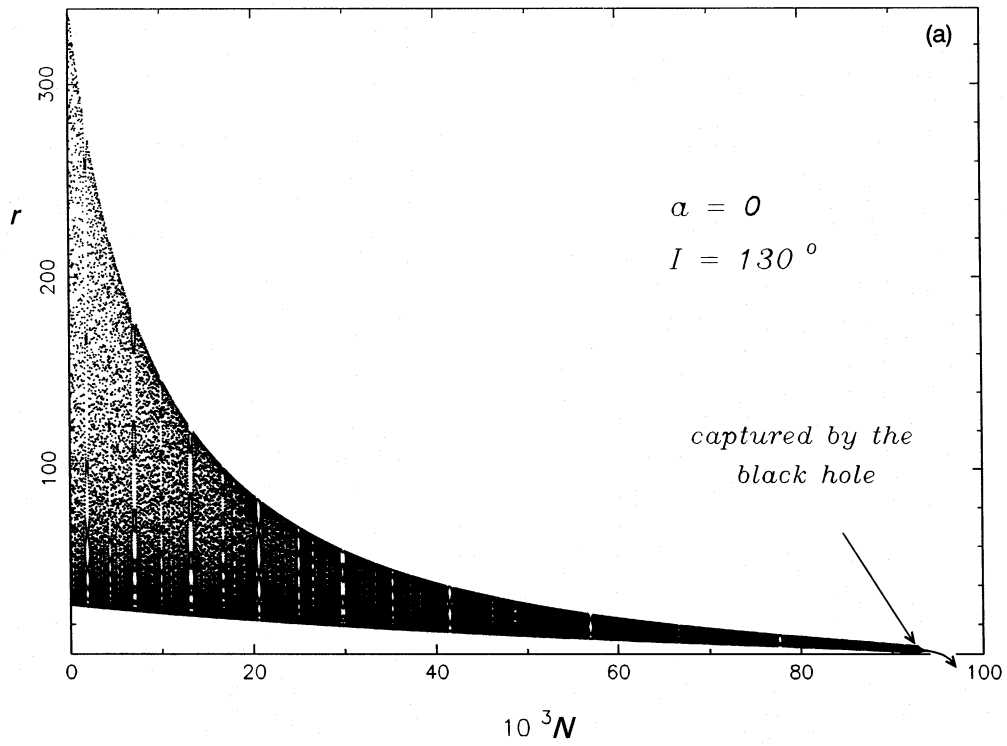

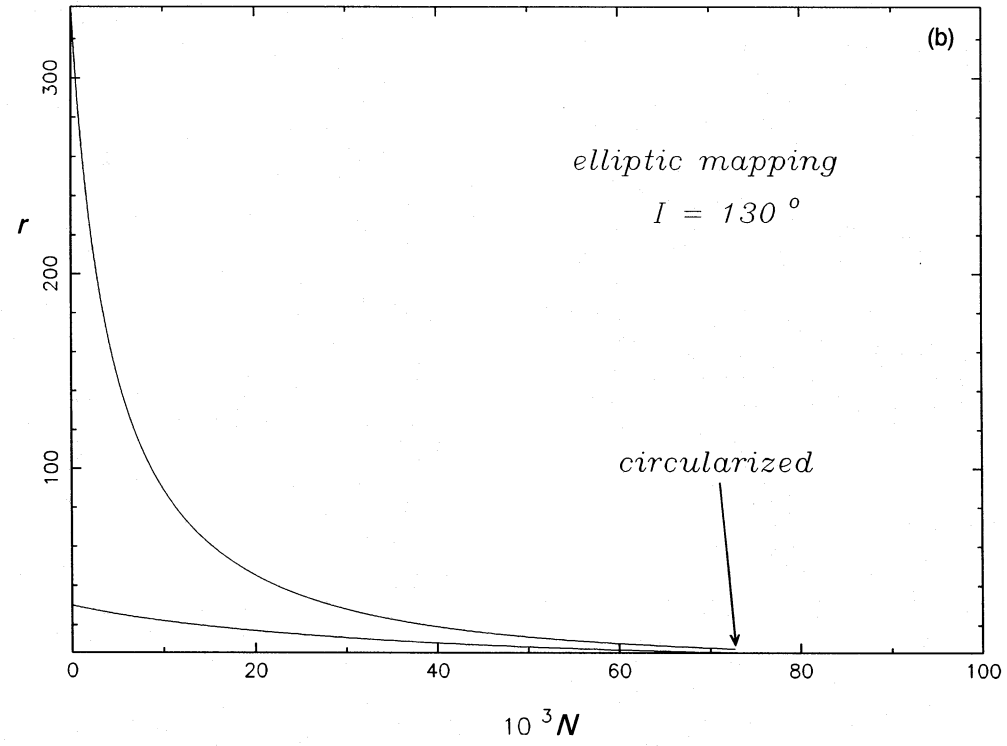

Figure 3. The graph (a) shows a similar orbit to those in Fig. 2, but now the initial trajectory is retrograde with an inclination of 130°. As commented upon in the text, it is captured by the central black hole. The graph (b) shows the 'Newtonian analogue' of (a). Only the 'adiabatic evolution' of the apocentre (upper curve) and the pericentre (lower curve) is seen, and there is no shift of pericentre.

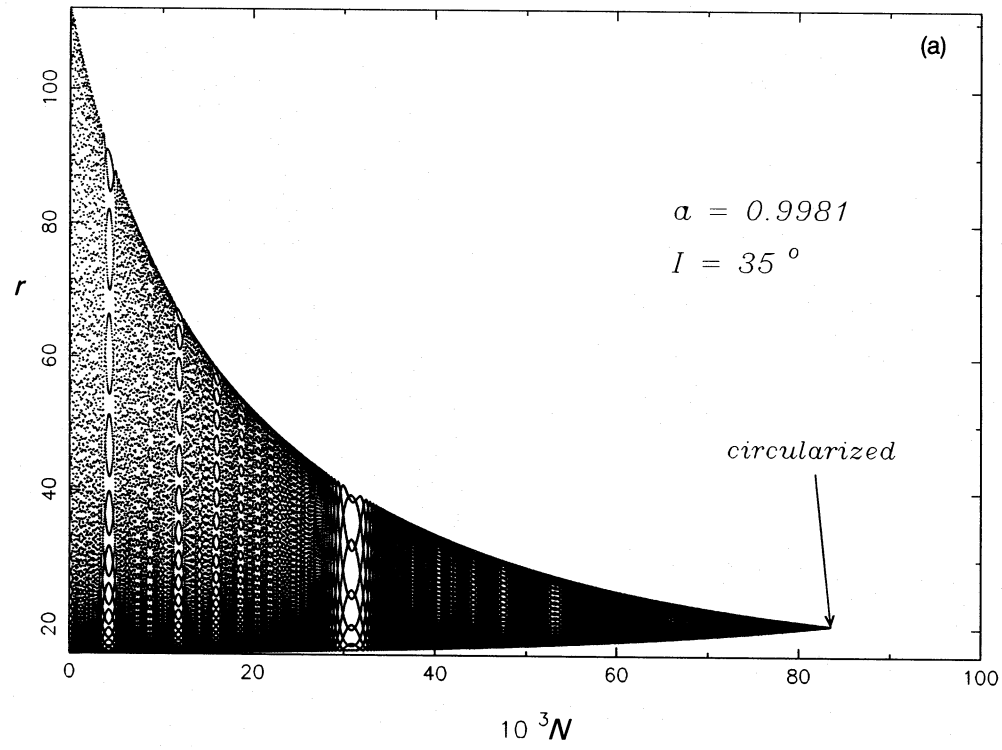

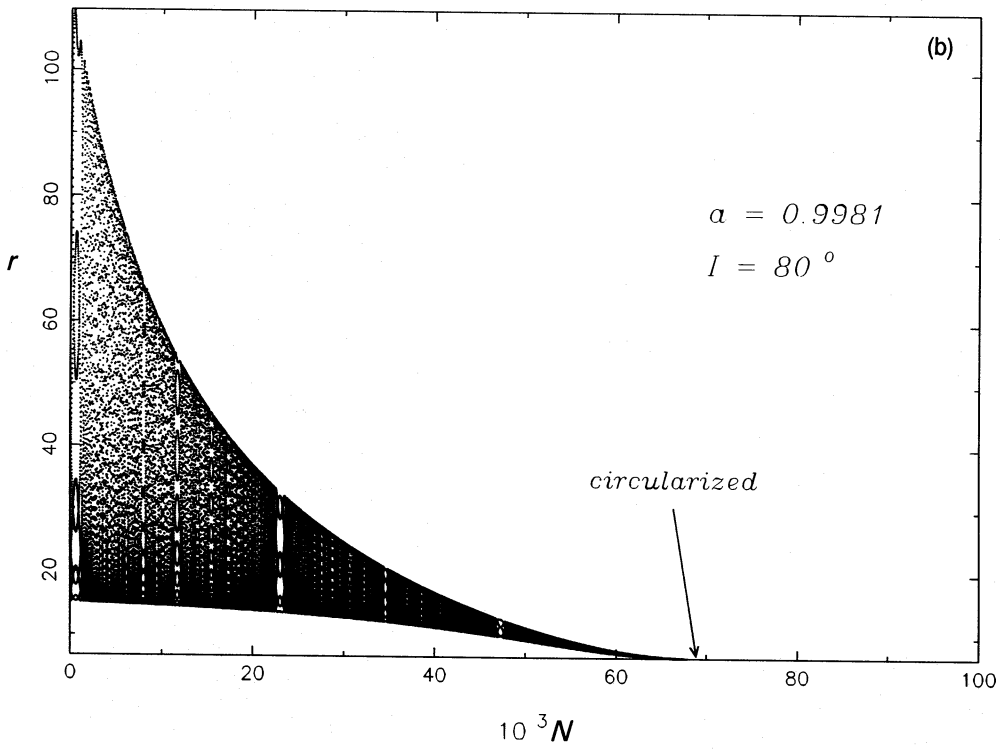

Figure 4. Orbits analogous to those in Fig. 2, but with a nearly extreme Kerr metric ($a=0.9981$). The initial pericentric distance is 15 (the same as for the Fig. 2 orbits if expressed in units of the gravitational radius of the central black hole). The initial inclinations are again chosen to be $I=35°$ (a) and $I=80°$ (b).

scenarios of AGN that require a rotating black hole. The second consequence is particularly important in describing the capture of the star into a bound orbit around the central black hole. Although many models assume a star to be located on such an orbit, the very process of the capture is not well understood.

ACKNOWLEDGMENTS

Our work was largely motivated by discussions with M. A. Abramowicz and by the work of Syer et al. (1991). We thank the unknown referee for very stimulating remarks, which helped us to improve the presentation of our work. We also acknowledge discussions with J. Bičák, P. Hadrava, A. Lanza, O. Semerák and R. Stark. VK acknowledges support from SISSA, Trieste. DV is grateful for the kind hospitality of CERGA, Grasse.

REFERENCES

Abramowicz M. A., 1992, in Holt S. S., Urry C. M., eds, Proc. 2nd Maryland Astrophys. Conf., Testing the AGN Paradigm. AIP, New York, p. 69
Abramowicz M. A., Bao G., Lanza A., Zhang X.-H., 1991, A&A, 245, 454
Abramowicz M. A., Lanza A., Spiegel E. A., Szuszkiewicz E., 1992, Nat, 356, 41
Bardeen J. M., 1973, in DeWitt C., DeWitt B. S., eds, Black Holes. Gordon and Breach, New York, p. 215
Bardeen J. M., Press W. H., Teukolsky S. A., 1972, ApJ, 178, 347
Byrd P. F., Friedman M. D., 1971, Handbook of Elliptic Integrals for Engineers and Scientists. Springer-Verlag, Berlin
Carter B., 1968, Phys. Rev., 174, 1559
Carter B., 1992, ApJ, 391, L67
Carter B., Luminet J.-P., 1983, A&A, 121, 97
Chandrasekhar S., 1983, The Mathematical Theory of Black Holes. Clarendon Press, Oxford
Cunningham C. T., Bardeen J. M., 1973, ApJ, 183, 237
D'Eath P. D., 1975a, Phys. Rev. D, 11, 1387
D'Eath P. D., 1975b, Phys. Rev. D, 12, 2183
Done C., Madejski G. M., Mushotzky R. F., Turner T. J., 1993, ApJ, 400, 138
Fabian A. C., Rees M. J., Stellar L., White N. E., 1989, MNRAS, 238, 729
Gradshteyn I. S., Ryzhik I. W., 1980, Table of Integrals, Series, and Products. Academic Press, New York
Gröbner W., Hofreiter N., 1965, Integraltafel, Erster Teil, Unbestimmte Integrale. Springer-Verlag, Vienna
Hills J. G., 1988, Nat, 331, 687
Karas V., Vokrouhlický D., 1993, ApJ, in press
Karas V., Vokrouhlický D., Polnarev A., 1992, MNRAS, 259, 569 (Paper I)
Kates R. E., 1980, Phys. Rev. D, 22, 1853
Kojima Y., 1991, MNRAS, 250, 629
Laor A., 1991, ApJ, 376, 90
Laor A., Netzer H., 1989, MNRAS, 238, 897
Lense J., Thirring H., 1918, Physik Z., 19, 156
Luminet J.-P., 1979, A&A, 75, 228
Luminet J.-P., Marck J.-A., 1985, MNRAS, 212, 57
Mittaz J. P. D., Branduardi-Raymont G., 1989, MNRAS, 238, 1029
Murray C. D., 1986, Icarus, 65, 70
Novikov I. D., Thorne K. S., 1973, in DeWitt C., DeWitt B. S., eds, Black Holes. Gordon and Breach, New York, p. 343
Novikov I. D., Pethick C. J., Polnarev A. G., 1992, MNRAS, 255, 276
Petrich L. I., Shapiro S. L., Stark R. F., Teukolsky S. A., 1989, ApJ, 336, 313
Press W. H., Teukolsky S. A., 1990, Comput. Phys., Jan/Feb, 92
Press W. H., Flannery B. P., Teukolsky S. A., Vetterling W. T., 1986, Numerical Recipes: The Art of Scientific Computing. Cambridge Univ. Press, New York
Rees M. J., 1993, in Ellis G. F. R., Lanza A., Miller J. C., eds, The Renaissance of General Relativity and Cosmology: A survey meeting to celebrate the 65th birthday of Dennis Sciama. Cambridge Univ. Press, Cambridge, in press
Sikora M., Begelman M. C., 1992, Nat, 356, 224
Stoghianidis E., Tsoubelis D., 1987, Gen. Relativ. Gravitation, 19, 1235
Suen W.-M., 1986, Phys. Rev. D, 34, 3633
Syer D., Clarke C. J., Rees M. J., 1991, MNRAS, 250, 505
Thorne K. S., 1974, ApJ, 191, 507
Thorne K. S., Hartle J. B., 1985, Phys. Rev. D, 31, 1815
Wallinder F. H., Kato S., Abramowicz M. A., 1992, A&AR, 4, 79
Wilkins D. C., 1972, Phys. Rev. D, 5, 814
Wisdom J., 1982, AJ, 87, 577
Zurek W. H., Siemiginowska A., Colgate S. A., 1992, in Holt S. S., Urry C. M., eds, Proc. 2nd Maryland Astrophys. Conf., Testing the AGN Paradigm. AIP, New York, p. 564

APPENDIX A: THE MAPPING ALGORITHM

This appendix outlines the explicit form of the mapping $(r, \phi; \eta)_i \to (r, \phi; \eta)_f$ from Section 2. Although our approach is straightforward, we believe that it has not yet been employed by other authors. As we found it very advantageous for practical purposes, we describe derivations relevant for this work in some detail. We constructed a numerical code, which employs efficient routines for evaluation of elliptic integrals and Jacobian elliptic functions (Press et al. 1986; Press & Teukolsky 1990). The code achieves better precision and about two orders of magnitude higher speed compared to direct numerical integration of the geodesic equation in its equivalent form of first-order differential equations. (We used direct integration to check the code.) The two cases, $0 < a < 1$ and $a = 0$, are technically somewhat different, and we discuss them separately.

A1 The case $0 < a < 1$

The steps to be followed are described below.

(i) Evaluate the latitudinal integral between two successive intersections with the equatorial plane:

$$I_\mu = \frac{2}{a\mu_+\sqrt{1-\mathscr{E}^2}} K(\mu_-/\mu_+), \tag{A1}$$

where $K(k)$ denotes the complete elliptic integral of the first kind.

(ii) Distinguish the three cases that may occur:

case I – four real roots of $R(r) = 0$, $r_4 < r < r_3$;
case II – four real roots of $R(r) = 0$, $r_2 < r < r_1$;
case III – two real and two complex roots of $R(r) = 0$, $r_2 < r < r_1$.

Denote $\eta_i = 1 (\eta_i = -1)$ if r is increasing (decreasing) at r_i; analogously, η_f for r_f.

(iii) Evaluate the increase of I_r between each pair of radial turning points:

$$\delta I_r = \begin{cases} \kappa K(k_1) & \text{(cases I and II)}, \\ \dfrac{2}{\sqrt{pq(1-\mathscr{E}^2)}} K(k_2) & \text{(case III)}, \end{cases} \tag{A2}$$

where

$$k_1 = \frac{(r_1-r_2)(r_3-r_4)}{(r_1-r_3)(r_2-r_4)}, \qquad k_2 = \frac{(r_1-r_2)^2-(p-q)^2}{4pq},$$

$$p^2 = (\chi_1 - r_1)^2 + \chi_2^2, \qquad q^2 = (\chi_1 - r_2)^2 + \chi_2^2,$$

$$\kappa = \frac{2}{\sqrt{(r_1-r_3)(r_2-r_4)(1-\mathscr{E}^2)}}.$$

(iv) Denote

$$f = \begin{cases} \kappa F(\varphi, k_1) & \text{(cases I and II)}, \\ \dfrac{1}{\sqrt{pq(1-\mathscr{E}^2)}} F(\varphi, k_2) & \text{(case III)}, \end{cases}$$

$$\tilde{I}_r = \begin{cases} m\delta I_r - \eta_f f & \text{if } \eta_f \eta_i > 0, \\ (m-\eta_f)\,\delta I_r + \eta_f f & \text{if } \eta_f \eta_i < 0. \end{cases} \tag{A3}$$

Here,

$$\sin^2\varphi = \begin{cases} \dfrac{(r_1-r_3)(r_i-r_4)}{(r_3-r_4)(r_1-r_i)} & \text{(case I)}, \\ \dfrac{(r_1-r_3)(r_i-r_2)}{(r_1-r_2)(r_i-r_3)} & \text{(case II)}, \end{cases}$$

$$\tan^2\frac{\varphi}{2} = \frac{p(r_i-r_2)}{q(r_1-r_i)} \qquad \text{(case III)};$$

$F(\varphi, k)$ is the incomplete elliptic integral of the first kind, and m is the number of turning points in r between the two successive intersections. In addition, one has to check whether the trajectory still remains above the horizon if the lower turning point is located below the horizon.

(v) The radial coordinate of the intersection is

$$r_f = \begin{cases} \dfrac{(r_1-r_3)r_4 + (r_3-r_4)r_1\sigma}{r_1 - r_3 + (r_3-r_4)\sigma} & \text{(case I)}, \\ \dfrac{(r_1-r_3)r_2 + (r_1-r_2)r_3\sigma}{r_1 - r_3 - (r_1-r_2)\sigma} & \text{(case II)}, \end{cases} \tag{A4}$$

with

$$\sigma = \mathrm{sn}^2(u, k_1)$$

and

$$u = \tfrac{1}{2}\sqrt{(r_1-r_3)(r_2-r_4)(1-\mathscr{E}^2)}\,(I_\mu - \tilde{I}_r),$$

or

$$r_f = \frac{qr_1\sigma + pr_2}{p + q\sigma} \qquad \text{(case III)}, \tag{A5}$$

with

$$\sigma = \frac{\mathrm{sn}^2(u, k_2)}{[1+\mathrm{cn}(u, k_2)]^2}$$

and

$$u = \sqrt{pq(1-\mathscr{E}^2)}\,(I_\mu - \tilde{I}_r).$$

Here, $\mathrm{sn}(u, k)$ and $\mathrm{cn}(u, k)$ are Jacobian elliptic functions. At this point, we are able to compute the r-coordinates of the intersections, which are sufficient to determine the evolution of eccentricity and inclination of the orbit and the number of revolutions before the trajectory is captured by the black hole or escapes to $\mathscr{E} \geq 1$ (and then presumably to infinity); ϕ-coordinates are also needed if we wish to study the precession. Finally, we need coordinate time to relate the revolutions to time as measured by a distant observer. In case III the orbit is in practice captured by the black hole after a few revolutions. Thus we exclude this case from further consideration.

(vi) Evaluate the following quantities.

Case I:

$$I_\pm = \kappa_\pm[(r_4-r_1)\,\Pi(\varphi, n_\pm, k_1) + (r_\pm - r_4)\,F(\varphi, k_1)] + \tilde{I}_\pm, \tag{A6}$$

$$n_\pm = \frac{(r_3-r_4)(r_\pm - r_1)}{(r_1-r_3)(r_\pm - r_4)},$$

$$J_r + 2K_r = \kappa r_4 \left[\left(\frac{r_4\alpha_1^4}{\alpha^4} + 2\frac{\alpha_1^2}{\alpha^2}\right) U + 2\frac{\alpha^2-\alpha_1^2}{\alpha^2} V_1 + 2r_4\alpha_1^2 \frac{\alpha^2-\alpha_1^2}{\alpha^4} V_1 + r_4 \frac{(\alpha^2-\alpha_1^2)^2}{\alpha^4} V_2\right] + \tilde{J}_r + 2\tilde{K}_r, \tag{A7}$$

with

$$U = F(\varphi, k_1), \qquad V_1 = \Pi(\varphi, -\alpha^2, k_1),$$

$$V_2 = \frac{1}{2(\alpha^2-1)(k_1^2-\alpha^2)}\left[\alpha^2 E(\varphi, k_1) + (2\alpha^2k_1^2 + 2\alpha^2 - \alpha^4 - 3k_1^2)\,V_1 + (k_1^2-\alpha^2)\,U - \mathrm{sn}(U, k_1)\,\mathrm{cn}(U, k_1)\,\mathrm{dn}(U, k_1)\frac{\alpha^4}{1-\alpha^2\mathrm{sn}^2(U, k_1)}\right],$$

$$\alpha^2 = \frac{r_4-r_3}{r_1-r_3}, \qquad \alpha_1^2 = \frac{r_1(r_4-r_3)}{r_4(r_1-r_3)},$$

$$\sin^2\varphi = \frac{(r_1-r_3)(r_i-r_4)}{(r_3-r_4)(r_1-r_i)},$$

$$\kappa_\pm = \frac{2}{(r_\pm - r_1)(r_\pm - r_4)\sqrt{(r_1-r_3)(r_2-r_4)(1-\mathscr{E}^2)}}.$$

Case II:

$$I_\pm = \kappa_\pm[(r_2-r_3)\,\Pi(\varphi, n_\pm, k_1) + (r_\pm - r_2)\,F(\varphi, k_1)] + \tilde{I}_\pm, \tag{A8}$$

$$n_{\pm}=\frac{(r_2-r_1)(r_{\pm}-r_3)}{(r_1-r_3)(r_{\pm}-r_2)},$$

$$J_r+2K_r=\kappa r_2\left[\left(\frac{r_2\alpha_1^4}{\alpha^4}+2\,\frac{\alpha_1^2}{\alpha^2}\right)U+2\,\frac{\alpha^2-\alpha_1^2}{\alpha^2}\,V_1 +2r_2\alpha_1^2\,\frac{\alpha^2-\alpha_1^2}{\alpha^4}\,V_1+r_2\,\frac{(\alpha^2-\alpha_1^2)^2}{\alpha^4}\,V_2\right]+\tilde{J}_r+2\tilde{K}_r, \tag{A9}$$

with U, V_1 and V_2 defined as above, and

$$\alpha^2=\frac{r_1-r_2}{r_1-r_3},\qquad \alpha_1^2=\frac{r_3(r_1-r_2)}{r_2(r_1-r_3)},$$

$$\sin^2\varphi=\frac{(r_1-r_3)(r_i-r_2)}{(r_1-r_2)(r_i-r_3)},$$

$$\kappa_{\pm}=\frac{2}{(r_{\pm}-r_3)(r_2-r_{\pm})\sqrt{(r_1-r_3)(r_2-r_4)(1-\mathscr{E}^2)}}.$$

$E(\varphi,k)$ and $\Pi(\varphi,n,k)$ are incomplete elliptic integrals of the second and the third kind, respectively, and $\mathrm{dn}(U,k)$ is a Jacobian elliptic function. Integration constants $\tilde{I}_{\pm}$, $\tilde{J}_r$ and $\tilde{K}_r$ are the values of the integrals in (15) and (17) evaluated between r_i and the last turning point. Thus they depend on the number of turning points in $r(m)$ and the sign of the initial radial velocity (η_i), and they can be given in terms analogous to equation (A3). We skip explicit expressions, because they are rather lengthy.

(vii) Finally,

$$J_{\mu}=\frac{2}{a\mu_+\sqrt{1-\mathscr{E}^2}}\,\Pi(-\mu_-^2,\mu_-/\mu_+), \tag{A10}$$

$$K_{\mu}=\frac{2r_1}{a\sqrt{1-\mathscr{E}^2}}\,[K(\mu_-/\mu_+)-E(\mu_-/\mu_+)], \tag{A11}$$

with $E(k)$ and $\Pi(n,k)$ being complete elliptic integrals of the second and the third kinds. Now we have all the necessary quantities for complete mapping of relevant trajectories in the Kerr metric.

A2 The Schwarzschild case ($a=0$)

We present the case of the Schwarzschild background metric separately, even though the general formalism developed for the Kerr metric can also be applied. The reason is two-fold. (i) The formulae valid for the general Kerr metric often include the angular momentum parameter a in the denominators (e.g. equations A10 and A11). These apparent singularities cancel out in the limit $a\to 0$, but they are the source of difficulties in numerical evaluation. (ii) As the symmetry of the space–time is now higher, and geodesics in the Schwarzschild metric remain always planar, we can avoid integration of the latitude θ, restricting ourselves to the current orbital plane of the test particle spanning one loop of the trajectory above/below the disc (the true orbital plane of the object is changed due to the interactions with the disc). Thus we reduce the order of the mapping by evaluating the integrals in polar coordinates in the orbital plane. The orbital plane differs from the disc plane by the current value of the inclination.

We consider the following coordinate systems: (i) Schwarzschild spherical coordinates (r,θ,ϕ); the latitude θ is measured from the axis of the disc plane and the polar angle ϕ is measured in the disc plane (the $\phi=0$ direction can be chosen arbitrarily); (ii) (r,ϑ) polar coordinates in the current orbital plane of the orbiting object, where the angle ϑ is measured from the actual nearest preceding apocentre of the unperturbed trajectory with the current orbital parameters. Let us clarify better the concept of the ϑ-origin, as it is intimately connected with our technique. The analytic integration of the geodesic motion in the Schwarzschild space–time is advantageously carried out if the polar angle in the orbital plane is measured from the nearest preceding apocentre. In each step of the mapping procedure, we are interested only in one orbital loop above/below the accretion disc; then the interaction with the disc changes the orbital parameters for the next loop. It is this orbital loop where the free motion of the test particle in the Schwarzschild background is applied. However, the orbital loop that is under consideration may not necessarily contain the apocentre of the orbit. Thus, apart from the true trajectory of the object, we introduce a reference trajectory of the object, with the same orbital parameters as the true one and coinciding with the true trajectory only on the current segment. This fictitious reference orbit defines the ϑ-origin – it is measured from the nearest preceding apocentre of the reference trajectory.

The equations of motion covering a single mapping step are as follows (e.g. Chandrasekhar 1983):

$$\vartheta_f-\vartheta_i(=\pi)=\int_{r_i}^{r_f}\frac{\mathrm{d}u}{U(u)^{1/2}}, \tag{A12}$$

$$t_f-t_i=\frac{\mathscr{E}}{\mathscr{L}}\int_{\vartheta_i}^{\vartheta_f}\frac{\mathrm{d}\vartheta}{u^2(1-2u)}, \tag{A13}$$

where

$$U(u)=2u^3-u^2+2\mathscr{L}^{-2}u-(1-\mathscr{E}^2)\,\mathscr{L}^{-2},$$

and $u=1/r$. Constants of motion are defined as $\mathscr{E}=-p_t$ and $\mathscr{L}=p_{\vartheta}$ (note that angular momentum $\mathscr{L}$ is defined with respect to the fictitious orbital plane, not with respect to the disc plane like Φ in the Kerr case). They are related to the tetrad components for the four-momentum in the locally static frames by means of equations (6) and (7). We define $I\equiv(\pi/2)-\beta$ as the inclination of the fictitious orbit with respect to the fixed reference disc plane (it can be equivalently expressed using the LNRF tetrad components in the equatorial plane: $\tan I=p^{\vartheta}/p^{\phi}$; cf. equation 8).

Again, we will concentrate on orbits characterized by $\mathscr{E}<1$ and $\mathscr{L}\neq 0$. The signs of the first and the last terms of the polynomial $U(u)$ guarantee at least one positive root of the equation $U(u)=0$ and, as $U(u=0)<0$, we conclude that this root corresponds to the apocentre of the orbit. The type of the orbit is determined by the properties of the other two roots of the equation $U(u)=0$. The roots cannot be real and negative at the same time (Chandrasekhar 1983). We exclude the possibility of multiple roots, as before. Hence we are left with the two kinds of orbit characterized by

(1) the three positive real roots of $U(u)=0$, which we arrange according to magnitude: $u_1<u_2<u_3$, and

(2) one positive real root (u_1) and two complex conjugated roots $(u_c,\overline{u_c})$ of $U(u)=0$.

The item (1) still encompasses two types of orbit: (i) those captured by the black hole in the sense that they have no pericentre above the horizon (the apocentre of such orbits is always less than 6, where the last stable orbit and presumably the inner edge of the accretion disc are located in the Schwarzschild case; hence we do not consider these orbits); (ii) quasi-elliptic orbits bound between the turning points, u_1 and u_2; we will call them case I orbits. In the terminology used by Chandrasekhar (1983), our case I orbits correspond to the orbits of the first kind. We call the case II orbits those of type (2) above. They have no pericentre, and fall unavoidably to the black hole (they correspond to the orbits with purely imaginary eccentricity in Chandrasekhar's terminology).

One can easily find a simple rule to distinguish both types of orbit: $\mathscr{L}^2<12$ implies the case II orbit. The case I orbits are characterized by $\mathscr{L}^2>12$ and, simultaneously,

$$(1-2u_*)(1+\mathscr{L}^2u_*^2)>\mathscr{E}^2,$$

where $u_*=1+|\mathscr{L}|^{-1}\sqrt{\mathscr{L}^2-12}$. In what follows, we will describe an algorithm for the mapping of these two types of orbit in detail. We will pay special attention to the case I orbits, as they will be shown to be the most important in astrophysical applications.

A2.1 Case I orbits

In close analogy to the Newtonian case, equation (A12) is advantageously integrated in terms of the relativistic 'true anomaly'

$$u(\chi)=\mu(1+e\cos\chi),$$

where

$$\mu=\frac{u_1+u_2}{2},\qquad e=\frac{u_2-u_1}{u_2+u_1}.$$

The quantity e can be interpreted as the eccentricity of the orbit. We do not write the explicit form of primitive functions obtained by integration (Chandrasekhar 1983), but we give formulae for the mapping that we need in our present work. After some manipulation, we arrive at the following form of the mapping:

$$u_{\rm f}=u_2-(u_2-u_1)\left[\frac{\sqrt{\Phi\Phi_\alpha}\sqrt{(1-k^2\Phi)(1-k^2\Phi_\alpha)}+\eta_{\rm i}\sqrt{\Psi\Psi_\alpha}}{1-k^2\Phi\Phi_\alpha}\right]^2, \tag{A14}$$

where now

$$\Phi=\frac{u_{\rm i}-u_1}{u_2-u_1},\qquad \Psi=\frac{u_2-u_{\rm i}}{u_2-u_1},$$

$$\Phi_\alpha=\mathrm{sn}^2\left(\frac{\pi}{2}\omega,k\right),\qquad \Psi_\alpha=\mathrm{cn}^2\left(\frac{\pi}{2}\omega,k\right),$$

$$\omega=\sqrt{1-2u_2-4u_1},\qquad k^2=2(u_2-u_1)\,\omega^{-2}.$$

Mapping of the sign function η is given as follows:

$$\eta_{\rm f}=\begin{cases}\mathrm{sgn}[\sigma(\chi_{\rm i})+\pi-\sigma(0)] & \text{if } \eta_{\rm i}=-1,\\ \mathrm{sgn}[\sigma(\chi_{\rm i})-\pi] & \text{if } \eta_{\rm i}=1,\end{cases} \tag{A15}$$

where

$$\chi_{\rm i}=\arccos(\Phi-\Psi),\qquad \chi\in\langle 0,\pi\rangle,$$

$$\sigma(\chi_{\rm i})=2\omega^{-1}F\left(\frac{\pi-\chi_{\rm i}}{2},k\right).$$

It is instructive to discuss the Newtonian limit of the mapping formula (A14) in which the terms proportional to some power of $1/c$ are neglected. This limit is now obscured by the fact that we imposed the widely used 'relativistic convention $c=1$', while now we want to suppress the terms containing c in the denominator. Careful book-keeping of c in the preceding equations suggests that the Newtonian limit corresponds to the fictitious procedure $\omega\to1$, $k\to0$. As a result, we obtain

$$u_{\rm f}=-u_{\rm i}+u_1^{\rm N}+u_2^{\rm N}, \tag{A16}$$

where the Newtonian boundaries are found to be

$$u_{1,2}^{\rm N}=\mathscr{L}^{-2}(1\pm\sqrt{1+2\mathscr{E}^{\rm N}\mathscr{L}^2}),\qquad \mathscr{E}^{\rm N}=\tfrac{1}{2}(\mathscr{E}^2-1)$$

(we retain the negative value for the Newtonian energy of bound orbits, as seen from the above definition of $\mathscr{E}^{\rm N}$). Equation (A16) is the correct expression for the 'elliptic' mapping. Formula (A16) is surprisingly simple, showing the linearity of the elliptic mapping. Moreover, we also have the simple rule $\eta_{\rm f}=-\eta_{\rm i}$. By contrast, the full relativistic mapping (A14) for the orbits of case I is highly non-linear, and the mapping in the u-coordinate is coupled with the mapping of the η-function due to $\eta_{\rm i}$ in equation (A14) and u in equation (A15).

Let us turn to equation (A13), describing the mapping in the t-coordinate. We start by expressing the indefinite integral on the right-hand side. Changing the ϑ-variable to χ according to the relation

$$\frac{\mathrm{d}\chi}{\mathrm{d}\vartheta}=-\omega\sqrt{1-k^2\cos^2(\chi/2)}\equiv-\omega\Delta(\chi,k),$$

one arrives at the primitive function

$$\begin{aligned}T(\chi)=\frac{2\mathscr{E}}{\omega\mathscr{L}}\Bigg[&\frac{2}{\mu(1-e)}\Pi\left(\frac{\pi-\chi}{2},\varepsilon^{-1},k\right)\\&+\frac{1}{[1-2\mu(1-e)]}\Pi\left[\frac{\pi-\chi}{2},\frac{4\mu e}{2\mu(1-e)-1},k\right]\\&+\frac{1}{2\mu^2(1-e^2)(1+\varepsilon k^2)}\Bigg\{\frac{\Delta(\chi,k)\sin\chi}{2[\varepsilon+\cos^2(\chi/2)]}\\&+[1+2\varepsilon(1+k^2)+3\varepsilon^2k^2]\,\varepsilon^{-1}\Pi\left(\frac{\pi-\chi}{2},\varepsilon^{-1},k\right)\\&+E\left(\frac{\pi-\chi}{2},k\right)-(1+\varepsilon k^2)\,F\left(\frac{\pi-\chi}{2},k\right)\Bigg\}\Bigg],\end{aligned} \tag{A17}$$

where

$$\varepsilon=\frac{u_1}{u_2-u_1}.$$

Now, the algorithm for evaluating the time-step associated with the mapping is as follows:

$\eta_i = -1$: introducing $\zeta_i = \mathrm{sgn}[\sigma(0) - \sigma(\chi_i) - \pi]$, we obtain

$$t_f - t_i = \begin{cases} T(\chi_f) - T(\chi_i) & \text{if } \zeta_i \geq 0, \\ 2T(0) - T(\chi_f) - T(\chi_i) & \text{if } \zeta_i < 0, \end{cases} \tag{A18}$$

where χ_f is determined by the relations

$$\begin{Bmatrix} \sin \\ \cos \end{Bmatrix} \chi_f = \begin{Bmatrix} \mathrm{sn} \\ \zeta_i \mathrm{cn} \end{Bmatrix} \left[\frac{\omega}{2} (\sigma(\chi_i) + \pi),\ k \right];$$

$\eta_i = 1$: introducing $\zeta_i = \mathrm{sgn}[\sigma(\chi_i) - \pi]$, we obtain

$$t_f - t_i = \begin{cases} T(\chi_i) - T(\chi_f) & \text{if } \zeta_i \geq 0, \\ T(\chi_i) + T(\chi_f) & \text{if } \zeta_i < 0, \end{cases} \tag{A19}$$

and now χ_f is determined by the relations

$$\begin{Bmatrix} \sin \\ \cos \end{Bmatrix} \chi_f = \begin{Bmatrix} \zeta_i \mathrm{sn} \\ \mathrm{cn} \end{Bmatrix} \left[\frac{\omega}{2} (\sigma(\chi_i) - \pi),\ k \right].$$

The Newtonian limit of equation (A18) is

$$t_f - t_i = \frac{2}{u_1^N u_2^N \mathscr{L}} \left[\frac{1}{\sqrt{1-e^2}} \arctan\left(\frac{\sqrt{1-e^2}}{e |\sin \vartheta_i|} \right) + \frac{e \sin \vartheta_i}{1 - e^2 \cos^2 \vartheta_i} \right], \tag{A20}$$

where

$$\cos \vartheta_i = \Phi - \Psi, \qquad \sin \vartheta_i = \eta_i \sqrt{1 - (\Phi - \Psi)^2},$$

and functions Φ and Ψ are defined as in (A14) and evaluated for $u_1 \equiv u_1^N$ and $u_2 \equiv u_2^N$.

A2.2 Case II orbits

These orbits have no pericentre. They are captured by the black hole in most cases, even though the interaction with the accretion disc can in principle modify the orbital parameters and change the type of the orbit. Consequently, we do not perform the mapping in full detail – we skip the derivation of the time interval $(t_f - t_i)$, which will not be needed for this type of orbit. We still need to describe the complete algorithm for the mapping in the u-coordinate and associated η-function. We were unsuccessful in finding a compact expression for the mapping $u_i \to u_f(u_i; u_1, u_c)$ similar to that presented in formula (A14), and thus in the following we give the algorithm of the mapping in several steps (well suited for programming).

(i) Evaluate the following quantities:

$$\mu = \tfrac{1}{4}(1 - 2u_1), \qquad e = \sqrt{3 - l(1 - l\mathscr{L}^{-2})},$$

$$\delta = \sqrt{(6\mu - 1)^2 + 4\mu^2 e^2}, \qquad \gamma_\pm = \delta \pm 6\mu - 1, \qquad k_\pm^2 = \frac{\gamma_\pm}{2\delta},$$

$$\varepsilon = \frac{4u_i + 2u_1 - 1}{e(1 - 2u_1)}, \qquad \varepsilon_c = \frac{1}{1 + \varepsilon^2},$$

$$\varepsilon_s = \begin{cases} \sqrt{1 - \varepsilon_c^2} & \text{if } u_i \geq \mu, \\ -\sqrt{1 - \varepsilon_c^2} & \text{if } u_i < \mu, \end{cases}$$

and the angle $\omega_i \in \langle -\pi/2, \pi/2 \rangle$, which is defined by

$$\sin^2 \omega_i = 1 - 2\gamma_+^{-1} \varepsilon_c [2e\mu\varepsilon_s + (6\mu - 1)\varepsilon_c],$$

where $\mathrm{sgn}(\omega_i) = \mathrm{sgn}(\varepsilon_s - k_-)$.

(ii) Exclude the captured trajectories by evaluating

$$\vartheta_i = [K(k_+) - F(\omega_i, k_+)]\, \delta^{-1/2};$$

the particle will be captured by the black hole before reaching the equatorial plane if $\vartheta_i \leq \pi$ and $\eta_i = -1$. Otherwise we continue to the following step.

(iii) Define

$$\lambda_* = F(\omega, k_+) - \eta_i \pi \delta^{1/2}, \qquad \zeta_i = \mathrm{sgn}[K(k_+) + \lambda_*],$$

and

$$\begin{Bmatrix} \kappa_s \\ \kappa_c \end{Bmatrix} = \begin{Bmatrix} \zeta_i \mathrm{sn}(\lambda_*, k_+) \\ \mathrm{cn}(\lambda_*, k_+) \end{Bmatrix}.$$

(iv) Finally, the mapping that we seek is given by

$$u_f = \mu(1 + e\mathscr{T}_{[\mathrm{sgn}(\kappa_s - \mathscr{S})]}), \qquad \eta_f = \zeta_i \eta_i, \tag{A21}$$

where we have used

$$\mathscr{T}_\pm = \gamma_+^{-1} \kappa_c^{-2} [2e\mu \pm \sqrt{4e^2\mu^2 + \gamma_+ \kappa_c^2 (\gamma_+ \kappa_s^2 - \gamma_-)}],$$

$$\mathscr{S} = -\sqrt{1 - 2(6\mu - 1)\gamma_+^{-1}}.$$

These orbits are unstable in the sense that they reach the singularity at $r = 0$, and thus in the Newtonian limit there are no analogous orbits corresponding to this case.

Equations (A14) and (A21) give the mapping for astrophysically interesting cases of geodesics in the Schwarzschild geometry.